5 min under argon, quenched with 5% aqueous HCl, worked up, and flash chromatographed with 5/95 ethyl acetate/hexane to yield 84 mg (42%) of di-5-hexenylmercury (**50**): ^{1}H NMR ($CDCl_3$) δ 1.05 (t, 4 H, J = 8.1 Hz), 1.45 (m, 4 H), 1.85 (m, 4 H), 2.05 (m, 4 H), 4.95 (m, 4 H), 5.80 (m, 2 H); ^{13}C NMR ($CDCl_3$) δ 28.30, 33.70, 34.68, 44.07, and 114.06 (CH_2), 139.33 (CH); IR 3075, 2921, 2845, 1640, 1458, 994, 908; MS (chemical ionization) m/e (relative intensity) 369 (7.5), 368 (6.7), 367 (27.0), 366 (15.1), 365 (19.8), 364 (13.5), 363 (7.1), 117 (100).

Acknowledgment. We gratefully acknowledge the donors of the Petroleum Research Fund, administered by the American Chemical Society, the Virginia Center for Innovative Technology, the Thomas F. Jeffress and Kate Miller Jeffress Memorial Trust Fund, and the National Science Foundation (Grant CHEM-9113448) for financial support.

Registry No. 6, 3481-02-5; **6**$^{\bullet-}$, 127793-45-7; **7**, 126525-21-1; **7**$^{\bullet-}$, 127909-63-1; **8**, 5685-43-8; **8**$^{\bullet-}$, 127793-46-8; **9**, 26921-44-8; **9**$^{\bullet-}$, 138354-12-8; **10**, 7143-76-2; **10**$^{\bullet-}$, 138354-13-9; **11**, 6921-45-5; **11**$^{\bullet-}$, 138354-14-0; **15a**, 138354-22-0; **15c**, 127793-52-6; **15d**, 138354-28-6; **16a**, 127793-49-1; **16b**, 127793-51-5; **17d**, 116215-96-4; **18a**, 138354-23-1; **18b**, 138354-15-1; **18c**, 138354-17-3; **18c**-d_{15}, 138354-19-5; **18d**, 138354-29-7; **19b**, 138354-16-2; **19c**, 138354-18-4; **19c**-d_{20}, 138354-20-8; **25**, 138354-21-9; **29**, 138354-24-2; **35**, 138354-25-3; **36**, 138354-26-4; **37**, 4160-52-5; **38**, 138354-27-5; **40**, 138354-30-0; **41**, 938-16-9; **41**$^{\bullet-}$, 54978-96-0; **42**, 2695-47-8; **43**, 16183-00-9; **45**, 23907-66-6; **47a**, 138354-33-3; **47b**, 138354-36-6; **48a**, 138354-32-2; **48b**, 138354-35-5; **49a**, 138354-31-1; **49b**, 138354-34-4; **50**, 39179-43-6; Δ^5-hexenylmercuric chloride, 63668-13-3.

Supplementary Material Available: DCV reaction order plots for decay of **6**$^{\bullet-}$, **7**$^{\bullet-}$, **8**$^{\bullet-}$, **10**$^{\bullet-}$, and **11**$^{\bullet-}$, plots for the determination of the apparent activation energy for decay of **6**$^{\bullet-}$, **7**$^{\bullet-}$, and **8**$^{\bullet-}$, plots of peak potential (E_p) vs log C_A and E_p vs ln ν for **8**, plots of $\nu_{0.5}$ vs ln ($1/\nu$) for decay of **6**$^{\bullet-}$, **7**$^{\bullet-}$, **8**$^{\bullet-}$, and **10**$^{\bullet-}$, predicted and observed mass spectral peak intensities for the coelectrolysis of **25** and **8**, results of Δ^5-hexenyl radical competition experiments using 1-bromo-5-hexene and 5-hexenylmercuric chloride as radical sources, and spectral data for **16b**, **18b,c**, **19b,c**, **18c**-d_{20}, and **19c**-d_{20} (11 pages). Ordering information is given on any current masthead page.

Design, Synthesis, and Kinetic Evaluation of a Unique Class of Elastase Inhibitors, the Peptidyl α-Ketobenzoxazoles, and the X-ray Crystal Structure of the Covalent Complex between Porcine Pancreatic Elastase and Ac-Ala-Pro-Val-2-Benzoxazole

Philip D. Edwards,*,†,‖ Edgar F. Meyer, Jr.,*,‡ J. Vijayalakshmi,‡ Paul A. Tuthill,† Donald A. Andisik,† Bruce Gomes,§ and Anne Strimpler§

Contribution from ICI Pharmaceuticals Group, A Business Unit of ICI Americas Inc., Wilmington, Delaware, 19897, and the Department of Biochemistry and Biophysics, Texas A&M University, College Station, Texas 77843-2128. *Received November 1, 1990*

Abstract: Peptidyl α-ketobenzoxazoles **1** and **2** are potent, competitive, reversible inhibitors of the serine proteinases HLE and PPE. These inhibitors were designed to inactivate the enzyme by interacting with both the serine hydroxyl group and the histidine imidazole ring of the catalytic triad. The X-ray crystal structure determination of **2** bound to PPE confirms the covalent attachment of the inhibitor's carbonyl carbon atom to the hydroxyl group of the active site Ser-195. The nitrogen atom of the benzoxazole ring participates in a hydrogen-bonding interaction with His-57. This is the first example of a reversible inhibitor designed to take advantage of the binding opportunities afforded by both the serine and the histidine of the catalytic triad in serine proteinases.

Introduction

Elastases (EC 3.4.21.11) are possibly the most destructive enzymes in the body, having the ability to degrade virtually all connective tissue components. Uncontrolled proteolytic degradation by elastases has been implicated in a number of pathological conditions. Pancreatic elastase can cause the fatal disease pancreatitis,[1] while leukocyte elastase has been implicated in acute respiratory distress syndrome,[2] rheumatoid arthritis,[3] atherosclerosis,[4] pulmonary emphysema,[5] and other inflammatory disorders.[6] Emphysema is believed to result from an imbalance between human leukocyte elastase (HLE)[7] and its endogenous inhibitor, α_1-proteinase inhibitor. One approach to controlling the progression of emphysema is to supplement the elastase inhibitor capacity of the lung with low molecular weight inhibitors of HLE. Peptidyl trifluoromethyl ketones,[8-10] peptidyl boronic acid esters,[11] and β-lactams[12] have emerged as leading candidates to demonstrate the utility of proteinase inhibitors for the treatment of emphysema.[13]

† Department of Medicinal Chemistry, ICI Pharmaceuticals Group.
‡ Department of Biochemistry and Biophysics, Texas A&M University.
§ Department of Pulmonary Pharmacology, ICI Pharmaceuticals Group.
‖ Address until June 1992: ICI Pharmaceuticals, Hurdsfield Industrial Estate, Macclesfield, Cheshire SK10 2NA, England.

(1) Geokas, M. C.; Rinderknecht, H.; Swanson, V.; Haverback, B. *J. Lab. Invest.* **1968**, *19*, 235-239.
(2) Burchardi, H.; Stokke, T.; Hensel, T.; Koestering, H.; Rahlf, G.; Schlag, G.; Heine, H.; Horl, W. H. *Adv. Exp. Med. Biol.* **1984**, *167*, 319-333.
(3) Janoff, A.; In *Neutral Proteases of Human Polymorphonuclear Leukocytes*; Havermann, K., Janoff, A., Eds.; Urban and Schwartzenberg: Baltimore, MD, 1978; pp 390-417.
(4) Janoff, A. *Annu. Rev. Med.* **1985**, *36*, 207-216.
(5) *Pulmonary Emphysema and Proteolysis: 1986*; Taylor, J. C., Mittman, C., Eds.; Academic Press, Inc: New York, 1987; pp 1-550.
(6) Stein, R. L.; Trainor, D. A.; Wildonger, R. A. *Annu. Rep. Med. Chem.* **1985**, *20*, 237-246.
(7) Abbreviations: HLE, human leucocyte elastase; PPE, porcine pancreatic elastase; Box, 2-benzoxazolyl; DBKA, peptidyl α,α-difluoro-β-keto amide; Ac, acetyl; Cbz, benzyloxycarbonyl; TFMK, trifluoromethyl ketone; TEA, triethylamine; THF, tetrahydrofuran; DMSO, dimethyl sulfoxide; WSCDI, 1-ethyl-3-[3-(dimethylamino)propyl]carbodiimide hydrochloride; HOBT, 1-hydroxybenzotriazole hydrate; TFA, trifluoroacetic acid; DMF, dimethylformamide; MeO, methoxy; Suc, succinyl; pNA, *p*-nitroanilide; rms, root mean square; FR, flow rate.
(8) Stein, R. L.; Strimpler, A. M.; Edwards, P. D.; Lewis, J. J.; Mauger, R. C.; Schwartz, J. A.; Stein, M. M.; Trainor, D. A.; Wildonger, R. A.; Zottola, M. A. *Biochemistry* **1987**, *26*, 2682-2689.

0002-7863/92/1514-1854$03.00/0

Scheme I. Synthesis of α-Ketobenzoxazole 1

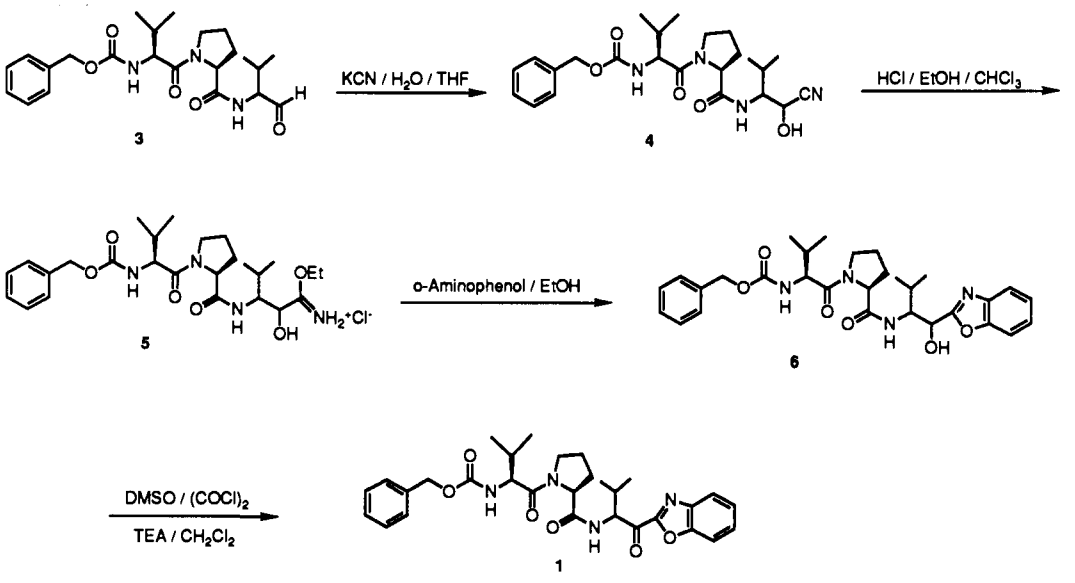

Scheme II. Synthesis of α-Ketobenzoxazole 2

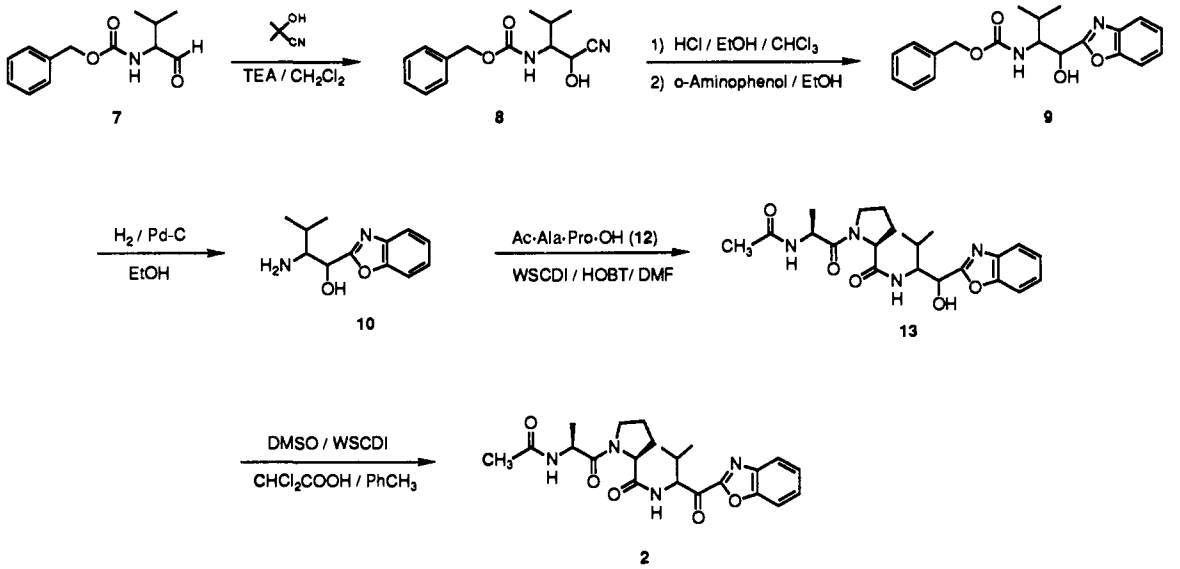

Our research efforts have focused on the development of mechanism-based[14] inhibitors of elastase, in particular peptidyl electrophilic ketones. A number of functional groups have been used to activate the carbonyl group of peptidyl ketones toward nucleophilic addition by the active site serine hydroxyl group of elastase, including the trifluoromethyl,[8-10] difluoromethylene,[9,15] halomethyl,[16] ester,[10,17] and keto[18,19] groups. We have found that a 2-benzoxazole ring positioned α to a ketone will also render the carbonyl group sufficiently electrophilic to react with the active site serine hydroxyl group. In addition, the benzoxazole ring participates in a unique interaction with the active site which is believed to contribute to the stability of the enzyme–inhibitor complex. We report herein the design, synthesis, and in vitro activity of the peptidyl α-ketobenzoxazoles Cbz-Val-Pro-Val-Box (**1**) and Ac-Ala-Pro-Val-Box (**2**).

To further investigate the nature of the interaction of this novel class of inhibitors with elastase, the structure of the complex of

(9) Imperiali, B.; Abeles, R. H. *Biochemistry* **1986**, *25*, 3760–3267.
(10) Peet, N. P.; Burkhart, J. P.; Angelastro, M. R.; Giroux, E. L.; Mehdi, S.; Bey, P.; Kolb, M.; Neises, B.; Schirlin, D. *J. Med. Chem.* **1990**, *33*, 394–407.
(11) Kettner, C. A.; Shenvi, A. B. *J. Biol. Chem.* **1984**, *259*, 15106–15114.
(12) Doherty, J. B.; Ashe, B. M.; Argenbright, L. W.; Barker, P. L.; Bonney, R. J.; Chandler, G. O.; Dahlgren, M. E.; Dorn, C. P., Jr.; Finke, P. E.; Firestone, R. A.; Fletcher, D.; Hagmann, W. K.; Mumford, R.; O'Grady, L.; Maycock, A. L.; Pisano, J. M.; Shah, S. K.; Thompson, K. R.; Zimmerman, M. *Nature* **1986**, *322*, 192–194.
(13) Trainor, D. A. *Trends Pharmacol. Sci.* **1987**, *8*, 303–307.
(14) The term *mechanism-based* has often been used to describe specifically inhibitors which are irreversible suicide inactivators of enzymes. Here it is used in a more general context to define inhibitors whose mode of action is based on the mechanism of enzymatic substrate hydrolysis, and which inactivate an enzyme by interacting with the catalytic residues within the active site. In addition to irreversible suicide inactivators, reversible and transition-state analogue inhibitors may be included in this definition.
(15) Trainor, D. A. Tenth American Peptide Symposium (Abstracts), Washington University, St. Louis, MO, 1987.
(16) (a) Powers, J. C. *Am. Rev. Respir. Dis.* **1983**, *127*, 554–558. (b) Rauber, P.; Angliker, H.; Walker, B.; Shaw, E. *Biochem. J.* **1986**, *239*, 633–640.
(17) Hori, H.; Yasutake, A.; Minematsu, Y.; Powers, J. C. In *Peptides, Structure and Function (Proceedings of the Ninth American Peptide Symposium)*; Deber, C. M., Hruby, V. J., Kopple, K. D., Eds.; Pierce Chemical Co.: Rockford, IL, 1985; pp 819–822.
(18) Stein, M. M.; Wildonger, R. A.; Trainor, D. A.; Edwards, P. D.; Yee, Y. K.; Lewis, J. J.; Zottola, M. A.; Williams, J. C.; Strimpler, A. M. In *Peptides, Chemistry, Structure, and Biology (Proceedings of the Eleventh American Peptide Symposium)*; Rivier, J. E.; Marshall, G. R., Eds.; ESCOM: Leiden, 1990; pp 369–370.
(19) Mehdi, S.; Angelastro, M. R.; Burkhart, J. P.; Koehl, J. R.; Peet, N. P.; Bey, P. *Biochem. Biophys. Res. Commun.* **1990**, *166*, 595–600.

2 and porcine pancreatic elastase (PPE) has been determined crystallographically to a resolution of 1.9 Å and has confirmed the productive, substrate-like binding of the α-ketobenzoxazole in the active site of PPE. The ketone carbonyl carbon atom is observed covalently attached to the hydroxyl group of Ser-195 with the benzoxazole nitrogen atom involved in a hydrogen-bonding interaction with His-57. Analogous complexes of PPE with a peptidyl TFMK (1.78-Å resolution)[20] and with a peptidyl α,α-difluoromethylene-β-keto amide (2.57-Å resolution)[21] have been reported. Details describing the structure–activity relationships within the series of peptidyl α-ketobenzoxazoles and the effect of other heterocyclic replacements will be reported elsewhere.[22]

Synthesis

The synthetic strategy employed to access the peptidyl α-ketobenzoxazoles is centered around the condensation of a nitrile with an aminophenol to form the heterocyclic ring (Scheme I). The nitrile required for the construction of α-ketobenzoxazole **1** was readily prepared from Cbz-Val-Pro-Val-H (**3**) and KCN/H_2O/THF. Treatment of cyanohydrin **4** with anhydrous HCl and ethanol in a Pinner reaction[23] afforded the intermediate imino ether hydrochloride **5**, which was cyclized with *o*-aminophenol to afford the α-hydroxybenzoxazole **6**.

A number of oxidants have been found to convert the hydroxybenzoxazoles into the corresponding ketones, including the Swern, Collins, Dess–Martin periodinane,[24] and Pfitzner–Moffatt oxidations. On balance, we have found the periodinane and Pfitzner–Moffatt oxidations the most generally useful. Due to the explosion hazard associated with periodinane and its byproducts,[25] we routinely use the Moffatt or Swern oxidations. Thus, treatment of **6** with oxalyl chloride/DMSO/TEA in methylene chloride afforded the peptidyl α-ketobenzoxazole **1**.

A more general sequence for assembling the peptide backbone of the α-ketobenzoxazoles is illustrated by the synthesis of ketone **2** (Scheme II). Aldehyde **7** can be converted to the cyanohydrin **8** with either KCN, trimethylsilyl cyanide/ZnI_2/CH_2Cl_2 or acetone cyanohydrin/TEA/CH_2Cl_2. The latter procedure is preferred with respect to safety of the reagents and purity of the crude product. Conversion of **8** to the hydroxybenzoxazole **9** followed by removal of the benzyloxycarbonyl protecting group affords the intermediate amino alcohol **10**, which can be coupled with peptide carboxylic acids to generate a variety of peptidyl α-hydroxybenzoxazoles. Thus, treatment of **10** with Ac-Ala-Pro-OH gave the alcohol **13**, which was converted to ketone **2** by the modified Moffatt oxidation of Gelb.[26]

Both ketones **1** and **2** exist as a 9:1 mixture of diastereomers epimeric at the carbon atom α to the ketone carbonyl group. This is the cumulative result of minor amounts of epimerization occurring during the preparation of the aldehyde, cyanohydrin formation, and oxidation to the ketone. Careful control of the reaction conditions can increase the ratio to greater than 95:5. The diastereomer ratio was determined by integration of the ^1H NMR resonance of the proton α to the ketone carbonyl at ~5 ppm.

Kinetic Assay

Reaction progress was measured spectrophotometrically by monitoring the release of *p*-nitroaniline at 410 nm during the enzymatic hydrolysis of MeO-Suc-Ala-Ala-Pro-Val-pNA. In a typical experiment, a cuvette containing 2.89 mL of buffer and 50 μL each of DMSO solutions of inhibitor and substrate was brought to thermal equilibrium in a jacketed holder in the cell compartment of the spectrophotometer. Reactions were initiated by the addition of enzyme and the values for K_i were calculated by standard methods from the velocities of the hydrolysis in the presence and absence of inhibitor.

For compounds **1**, **2**, and **15**, the progress curves were linear with a slope greater than zero, indicating that enzyme and inhibitor were equilibrated and that inhibition was reversible. Lineweaver–Burk plots derived from separate sets of reaction progress curves in which the substrate concentration was varied at fixed inhibitor and enzyme concentrations showed compounds **1** and **15** to be competitive inhibitors of HLE at pH 7.8, and compound **2** to be a competitive inhibitor of PPE at pH 5.0.

Table I. Optimum and Refined Values for the Geometrical Parameters at the Covalent Region between the Inhibitor and Ser-195 in the Active Site

geometric parameters	optimum	refined
Bond Length, Å		
Ser C_β–Ser O_γ	1.415	1.41
Val C′–Ser O_γ	1.46	1.45
Val C_α–Val C′	1.54	1.51
Val C′–Val O	1.36	1.37
Val C′–Box C1	1.54	1.52
Bond Angle, deg		
Val C′–Ser O_γ–Ser C_β	115.3	116.1
Val C_α–Val C′–Ser O_γ	109.0	107.8
Val C_α–Val C′–Val O	109.0	109.7
Val C_α–Val C′–Box C1	109.0	109.7
Ser O_γ–Val C′–Box C1	109.0	111.3
Val O–Val C′–Ser O_γ	109.0	110.4

Crystallographic Data Collection

Commercially available PPE was used. Crystals were obtained, using a solution of PPE in 0.1 M sodium phosphate buffer at pH 5.0 with the enzyme concentration of 1.2% (w/v), by vapor diffusion from 0.1 M sodium phosphate and 0.1 M sodium sulfate solution. The crystals belonged to space group $P2_12_12_1$ with cell dimensions 51.13 Å, 58.13 Å, 75.38 Å. A large (0.4 × 0.4 × 0.4 mm) crystal of elastase (PPE) was mounted in a 0.5-mm capillary with excess inhibitor and allowed to soak for 3 days. Data collection was initiated on a FAST area detector using Ni-filtered Cu Kα radiation (the Rigaku Ru200 generator operating at 120 mA and 45 kV), with a scan range of 0.1°/step and a rate of 100 s/step. Data were collected over a rotation range of −2 to +92°. The crystal was rotated 30° about the direct-beam axis (ROTZ) and an additional 40° scan of data was measured. These two data sets were divided into separate files comprising 5.5° wedges. These files were scaled and merged using the PROTEIN[29] system. The final RMERGE value [defined as $\sum|(I_{(i)} - \langle I\rangle|/\sum I_{(i)}$, $I_{(i)}$ being the intensity value of an individual measurement and $\langle I\rangle$ the corresponding mean value, the summation being over all data sets common to both the measurements] was 6.2%. The data were 55% complete to 1.9 Å; the final shell, from 1.93 to 1.90 Å, was 41% complete. The total number of reflections collected was 10180.

Refinement. The data were processed and the refinements carried out using the program TNT.[30] The isomorphous native PPE coordinates (R = 16.9% for 1937 atoms, including 117 waters of hydration) were initially taken as the starting set for calculating structure factors, F_c's. The initial R factor was 33% with these F_c's and observed structure factors, F_o's, for the complex. Initially, 20 cycles of refinements involving alternately 3 cycles of positional and 1 cycle of temperature factor refinement were calculated to account for scale differences and small differences in cell dimensions between the native and the complex structures. At this point the R factor was 25%. Phased on the native structure coordinates, a difference Fourier map was calculated. Ser-195 was made "dummy" and thus did not contribute to F_c's. The density found in the active site clearly indicated that a complex had been formed. Also, the continuous density from O_γ of Ser-195 indicated covalent binding of the inhibitor with O_γ of Ser-195. The inhibitor was modeled to fit the electron density in the active site. The positions of sulfate and calcium ions were found to have the same loci as in the native structure and most of the water molecules were close to positions found in the native structure. The modeled inhibitor was included in further cycles of refinement; an initial tempera-

(20) Takahashi, L. H.; Radhakrishnan, R.; Rosenfield, R. E., Jr.; Meyer, E. F., Jr.; Trainor, D. A.; Stein, M. *J. Mol. Biol.* **1988**, *201*, 423–428.
(21) Takahashi, L. H.; Radhakrishnan, R.; Rosenfield, R. E., Jr.; Meyer, E. F., Jr.; Trainor, D. A. *J. Am. Chem. Soc.* **1989**, *111*, 3368–3374.
(22) Manuscript for submission to *J. Med. Chem.*, in preparation.
(23) Neilson, D. G. In *The Chemistry of Amidines and Imidates*; Patai, S., Ed.; John Wiley & Sons: New York, 1975; pp 385–489.
(24) Dess, D. B.; Martin, J. C. *J. Org. Chem.* **1983**, *48*, 4155–4156.
(25) Plumb, J. B.; Harper, D. J. *Chem. Eng. News* **1990**, *68* (July 16), 3.
(26) Fearon, K.; Spaltenstein, A.; Hopkins, P. B.; Gelb, M. H. *J. Med. Chem.* **1987**, *30*, 1617–1622.
(27) Swanson, S. M. *Acta Crystallogr.* **1988**, *A44*, 437–442.
(28) Luzatti, V. *Acta Crystallogr.* **1952**, *5*, 802–810.
(29) Steigemenn, W. Ph.D. Thesis, T. U. Munchen, 1974.
(30) Tronrud, D. E.; Lynn, F.; Ten Eyck, L. F.; Matthews, B. W. *Acta Crystallogr.* **1987**, *A43*, 489–501.

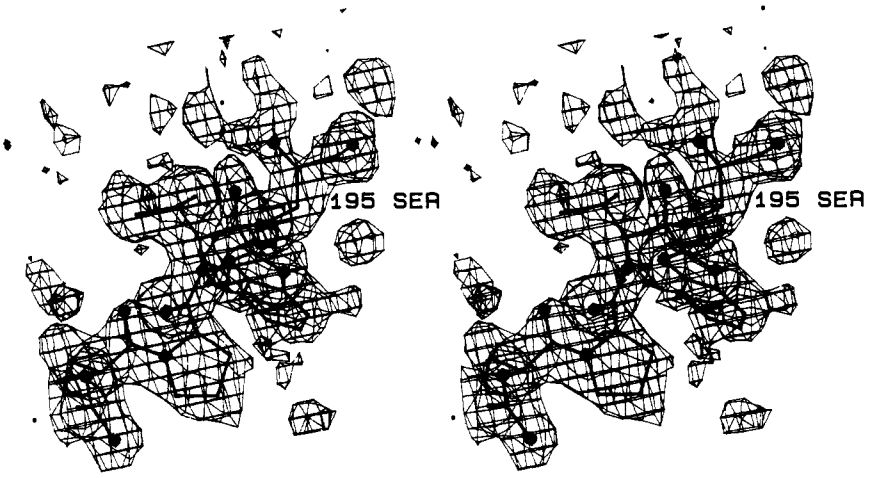

Figure 1. Stereoview of the unbiased ("omit") difference Fourier map of the active site of the enzyme–inhibitor complex. Electron density contours at 0.2 e/Å^3 (0.8σ) define an envelope that contains that or higher electron density, as well as all atoms of the Ser-195 and the inhibitor.

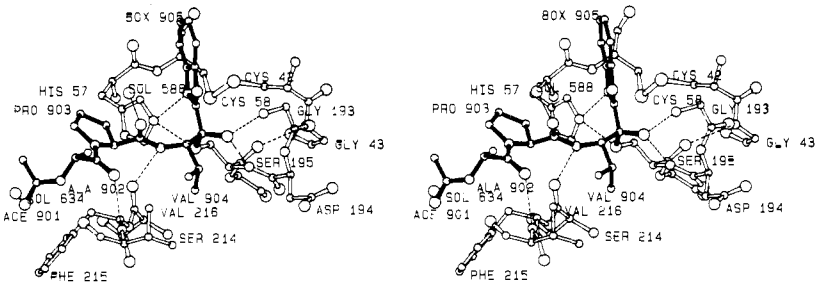

Figure 2. Stereoview of the active site region, drawn by Program Ballstick (R. Radhakrishnan, unpublished) showing covalent and hydrogen bonds of the title complex.

Table II. Optimum and Refined Values for the Geometrical Parameters of the Benzoxazole Ring in the Inhibitor

geometric parameters	optimum	refined	geometric parameters	optimum	refined
		Bond Length, Å			
C1–N2	1.32	1.32	C6–C7	1.375	1.38
N2–C3	1.40	1.39	C7–C8	1.40	1.40
C3–C4	1.40	1.40	C8–O9	1.36	1.35
C4–C5	1.375	1.38	O9–C1	1.35	1.35
C5–C6	1.40	1.41			
		Bond Angle, deg			
C–C1–O9	118.0	115.7	C7–C8–C3	120.0	120.3
C1–N2–C3	104.0	102.8	O9–C8–C3	107.0	106.8
C3–C4–C5	120.0	119.9	C8–O9–C1	105.0	105.3
C4–C5–C6	120.0	120.5	O9–C1–N2	114.0	115.1
C5–C6–C7	120.0	119.9	N2–C3–C8	110.0	109.4
C6–C7–C8	120.0	120.5	C4–C3–C8	120.0	119.7

ture factor of 20 Å^2 was assigned to all non-hydrogen atoms of the inhibitor. Refinement was calculated alternately with three cycles on positional parameters and one cycle of temperature factor refinement. Geometry constraints were introduced during positional coordinate refinements which involve both the X-ray module and the geometry module. In the geometry module a weight of 0.001 for the R factor, 1.0 for the bond length, 3.0 for bond angles, 10.0 for contact distance, and 10.0 for group planarity were given in the refinements. The parameters specified for the geometry near the covalent linkage are given in Table I. Program default geometric parameters were employed for the peptidyl portion of the inhibitor. The geometry of the benzoxazole ring was derived from small-molecule structure information from the Cambridge Crystal Data Base.[31] The geometric values used for the benzoxazole ring are given in Table II. The option of solvent contribution in TNT was utilized at the later stages of refinements when all discernible water molecules had been introduced. A total of 380 cycles of refinements reduced the R factor ($R = \sum|F_o| - |F_c|/\sum|F_o|$) to 0.162. The final standard deviation in bond length was 0.012 Å for 1904 bond lengths and 1.6° for 2598 bond angles. The overall temperature factor weighted as per the electron count for the inhibitor was 16.2 Å^2 for 31 inhibitor atoms and 15.0 Å^2 for 2018 atoms in the protein. The final refinement statistics are given in Table III.

Table III. Crystallographic Parameters and the Final Refinement Statistics for the Structure of the Complex of PPE with Acetyl-Ala-Pro-Val-2-benzoxazole

crystal size, mm	0.4 × 0.4 × 0.4
cell dimensions, Å	a = 51.13, b = 58.13, c = 75.38
data collection temp, °C	19
resolution range of data, Å	30.0–1.9
space group	$P2_12_12_1$
effective resolution, Å[27]	2.0
no. of atoms/asymmetric unit	2049
no. of unique reflections	10180
R factor ($R = \sum\|\|F_o\| - \|F_c\|\|/\sum\|F_o\|$)	0.162
overall temp factor of 2018 atoms in protein weighted as per electron count, Å^2	15.0
overall temp factor of the 31 inhibitor atoms, Å^2	16.2
σ of 1904 bond lengths, Å	0.012
σ of 2598 bond angles, deg	1.6
features of final residual difference density map, e/Å^3	
min height	−0.40
max height	0.45
σ	0.09
mean positional error, Å[28]	0.2

Results

The peptidyl α-ketobenzoxazole **1** is a potent inhibitor of HLE (K_i = 3.0 × 10^{-9} M at pH 7.8). The kinetic analysis is consistent with reversible inhibition, while Lineweaver–Burk plots demonstrated that inhibition of HLE was competitive as well. Compound **2** is a reversible inhibitor of both HLE (K_i = 7.3 × 10^{-8} M at pH 7.8) and PPE (K_i = 2.8 × 10^{-7} M at pH 7.8 and 6.2 × 10^{-6} M

(31) Allen, F. H.; Bellard, S.; Brice, M. D.; Cartwright, B. A.; Doubleday, A.; Higgs, H.; Hummelink, T.; Hummelink-Peters, B. G.; Kennard, O.; Motherwell, W. D. S.; Rodgers, J. R.; Watson, D. G. *Acta Crystallogr.* **1979**, *B35*, 2331–2339.

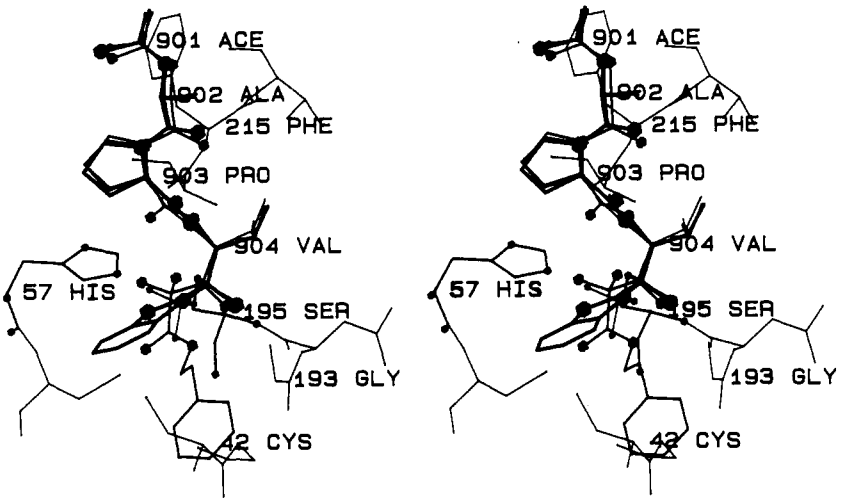

Figure 3. Stereoview of the superimposed models of the peptidyl TFMK (light lines), DBKA (medium lines), and α-ketobenzoxazole complex (heavy lines). It is noteworthy that the independently determined peptidyl moieties are virtually identically situated in the extended (S_3–S_1) binding site of PPE. The BLOB option (A. Karrer, unpublished) to program FRODO is used to indicate heteroatoms.

Table IV. Hydrogen Bonds (Å) in the Active Site of the Complex

Ace O···Sol-634 OH	3.20
Ala NH···Val-216 O	2.59
Ala O···Val-216 NH	2.89
Pro O···Sol-588 OH	2.48
Val O···Gly-193 NH	2.65
Val O···Ser-195 NH	2.56
Gly-43 NH···Ser-195 O	2.82
His-57 N_ϵ2H···Ser-195 O_γ	3.05
His-57 N_ϵ2H···Box-905 N2	2.81

at pH 5.0) and was shown to be a competitive inhibitor of PPE at pH 5.0. In contrast to peptidyl TFMKs and α-keto esters, the peptidyl α-ketobenzoxazoles are not slow-binding inhibitors[32] of serine proteinases.

The X-ray analysis shows unambiguously the hemiketal linkage of the carbonyl carbon atom of the valine residue of the inhibitor to O_γ of Ser-195 in the active site region. The original unbiased difference Fourier map had continuous electron density corresponding to the covalent linkage. The electron density for the inhibitor as bound to the enzyme is given in Figure 1. The density clearly indicated tetrahedral geometry around the carbonyl carbon atom forming the covalent bond. Figure 2 shows the final model of the inhibitor bound to the enzyme with the hydrogen-bonding scheme.

The productive, substrate-like binding of peptidyl inhibitors in the forward direction is characterized by an antiparallel β-pleated sheet arrangement of the inhibitor with the enzyme. There are also instances of nonproductive backward bindings in noncovalent peptide complexes in which the inhibitor forms a parallel β-pleated sheet with the enzyme.[33] This analysis confirms the productive forward binding mode and hemiketal linkage of the peptidyl α-ketobenzoxazoles.

There are six hydrogen bonds between the inhibitor and the enzyme. Two water molecules in the active site also participate in the hydrogen-bonding interactions. The hydrogen-bonding distances between donor and acceptor atoms are summarized in Table IV. The carbonyl oxygen atom of valine at the P_1 position[34] of the inhibitor is pointing toward the "oxy anion" hole forming hydrogen bonds with the amido nitrogen atoms of Gly-193 (2.65 Å) and Ser-195 (2.56 Å). The amido nitrogen atom of valine does not appear to be involved in a significant interaction with the carbonyl oxygen atom of Ser-214 since neither the distance (3.3 Å) nor the directionality are appropriate for a favorable hydrogen bond. This hydrogen bond is similarly lacking in other oligopeptide complexes with serine proteinases.[21] The proline residue at P_2 does not form any hydrogen bonds with the enzyme and does not contribute to the β-pleated sheet arrangement. The pyrrolidine ring points toward solution and does not interact with the S_2 pocket. The P_3 alanine residue of the inhibitor contributes to the antiparallel β-pleated sheet interaction and is involved in two hydrogen bonds to the enzyme, one between its carbonyl oxygen atom and the amido nitrogen atom of Val-216 (2.89 Å) and the other between its amido nitrogen atom and the carbonyl oxygen atom of Val-216 (2.59 Å). N_ϵ2 of His-57 makes a bifurcated hydrogen bond with the nitrogen atom of the benzoxazole ring (2.81 Å) and O_γ of Ser-195 (3.05 Å).

The isopropyl side chain of the P_1 valine fits the S_1 subsite well, making van der Waals interactions with hydrophobic groups in the S_1 subsite (Thr-213, Val-216, Thr-226, Val-227). The P_3 methyl group lies in the S_3 pocket, which is a shallow depression on the surface of the enzyme formed by residues Val-216, Arg-217A, Gly-219, and Gln-192. The S_4 pocket of the enzyme is partially blocked by a symmetry-related molecule. As a result, complexes of PPE with inhibitors larger than tripeptides cannot be generated in the solid state by the current experimental conditions.

The imidazole ring of His-57 is found in the "in" position characteristic of the native enzyme as well as in PPE complexed with peptide substrates and inhibitors. This may be contrasted with the His-57 imidazole ring in the "out" position, as exhibited in most heterocyclic inhibitor complexes [e.g., ref 35 and as discussed in ref 36 (cf. Figure 9 of ref 36)]. The root mean square (rms) deviation between the native enzyme and the title structure for 747 backbone atoms (NCCO) is 0.17 Å (0.07). Compared with the previously solved analogous structure of a peptidyl trifluoromethyl ketone complexed with PPE,[20] the rms deviation is 0.19 Å (0.07) for 757 common backbone atoms, and for 755 backbone atoms of the peptidyl α,α-difluoromethylene-β-keto amide–PPE complex,[21] it is 0.15 Å (0.06) compared with the title complex. The peptide backbone conformations of the inhibitors in all three structures are also the same. These differences are within the precision of the analyses of free and complexed PPE, indicating minimal conformational change upon ligand binding:

(32) (a) Morrison, J. F.; Walsh, C. T. *Adv. Enzymol.* **1988**, *61*, 201–301. (b) Rich, D. H.; Northrop, D. R. In *Computer Aided Drug Design, Methods and Applications*; Perun, T. J., Propst, C. L., Eds.; Marcell Dekker, Inc.: New York, 1989; pp 185–250.

(33) (a) Shotton, D. M.; White, N. J.; Watson, H. C. *Cold Spring Harbor Symp. Quant. Biol.* **1972**, *36*, 91–105. (b) Hughes, D. L.; Sieker, L. C.; Bieth, J.; Dimicoli, J. L. *J. Mol. Biol.* **1982**, *162*, 645–658. (c) Meyer, E. F., Jr.; Radhakrishnan, R.; Cole, G. M.; Presta, L. G. *J. Mol. Biol.* **1986**, *189*, 533–539.

(34) Schechter, I.; Berger, A. *Biochem. Biophys. Res. Commun.* **1967**, *27*, 157–162.

(35) Powers, J. C.; Oleksyszyn, J.; Lakshmi Narasimhan, S.; Kam, C.-M.; Radhakrishnan, R.; Meyer, E. F., Jr. *Biochemistry* **1990**, *29*, 3108–3118.

(36) Bode, W.; Meyer, E. F., Jr.; Powers, J. C. *Biochemistry* **1989**, *28*, 1951–1963.

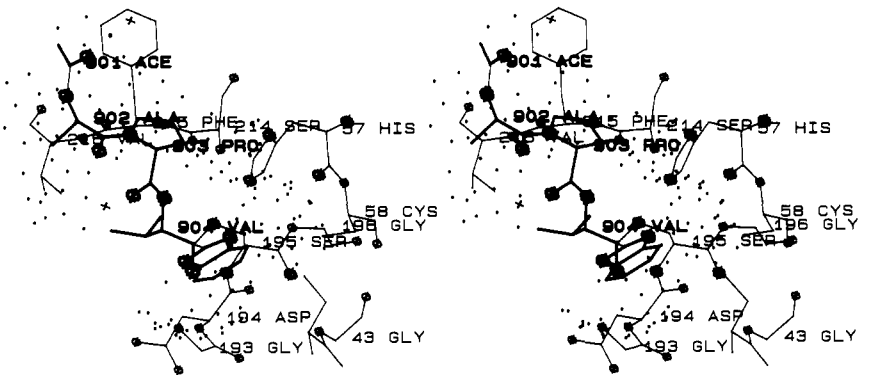

Figure 4. Stereoview of the title complex illustrating the van der Waals contact surface of the inhibitor (heavy lines) + enzyme (light lines) complex. Most enzyme atoms are seen to be on or beyond the contact surface. The noticeable exception is the $N_\epsilon 2$ of the imidazole ring of His-57, which penetrates the contact surface to make a hydrogen bond to the inhibitor (cf. Figure 2 and Table IV). The displayed contact surface is provided by the INTER command of program FRODO,[46] with input parameters set to locate points on a double van der Waals radius surface that are at least 2 Å from the inhibitor.

thus PPE can be considered a "lock and key" enzyme.[37] Figure 3 shows a comparative display of the three analogous peptidyl inhibitors as bound to the enzyme in the active site.

Figure 4 presents the van der Waals surface interactions between receptor and ligand in the active site. The contact surface is sparsely dotted, pictorially describing those regions of the inhibitor in direct contact with the enzyme and those out of contact. The surface contact of His-57 imidazole ring (still hydrogen bonded to Ser-195), Gln-192, and the antiparallel β-sheet from Ser-214 to Ser-217A forms a tight receptor pocket for the ligand.

Discussion

The peptidyl α-ketobenzoxazoles evolved from the concept that a heterocyclic ring possessing an electron-withdrawing inductive effect could activate an adjacent ketone carbonyl group toward nucleophilic addition. It was envisioned that a heterocycle positioned at the C-terminal end of an appropriate substrate-like peptide might afford mechanism-based inhibitors of serine proteinases in which the carbonyl carbon atom becomes covalently attached to the active site serine hydroxyl group. Additionally, incorporating into the heterocyclic ring a heteroatom capable of functioning as a hydrogen bond acceptor might further stabilize the hemiketal adduct through formation of a hydrogen bond with the protonated active site His-57. These design goals have been realized with the α-ketobenzoxazoles.

Simple tripeptidyl α-ketobenzoxazoles are very potent inhibitors of elastase. Cbz-Val-Pro-Val-Box (**1**) inhibits HLE with a K_i of 3.0×10^{-9} M. Table V lists the inhibition constants against HLE for a number of peptidyl electrophilic carbonyl-based inhibitors. It can be seen that α-ketobenzoxazole **1** is more potent than methyl ketone **17** and aldehyde **3** and has a potency which approaches that of the corresponding trifluoromethyl ketone **18**. Consistent with the proposed mechanism of inhibition of **1**, the hydroxybenzoxazole **6**, which is not capable of forming a covalent attachment to Ser-195, is almost 10 000-fold less potent than **1**.

These results, however, were not obvious at the outset of our investigation. In contrast to aldehydes and fluorinated ketones, an aromatic α-ketoheterocycle would be expected to exist as a conjugated, coplanar system. In order to form a tetrahedral adduct with the enzyme active site serine hydroxyl group, this resonance-stabilized system would have to be disrupted. Therefore, the expectation would be that an α-ketoheterocycle would *not* be an effective inhibitor of serine proteinases. Indeed, while a large number of CBZ-Val-Pro-Val-heterocycles were investigated for their ability to inhibit HLE,[22] only a few had a K_i less than 10^{-7} or 10^{-6} M. On the basis of the inhibition constant of the hydroxybenzoxazole **6**, this level of potency is about that expected for an inhibitor which binds to the extended binding pocket of the enzyme but does not form a stable covalent bond. The benzoxazole ring was chosen for further studies because it was found to possess both a high level of potency and adequate stability. *This represents the first example of a heterocyclic ring system functioning as an integral part of a stable, fully reversible, mechanism-based inhibitor of a serine proteinase.* All other heterocycles which have been reported as inhibitors of serine proteinases either do not interact with the active site of the enzyme, irreversibly inactivate the enzyme, or are themselves destroyed during the activation process.

We initiated these studies with an investigation of benzoxazole and oxazoline heterocycles because they possess a nitrogen atom capable of functioning as a hydrogen bond acceptor. Upon formation of the tetrahedral intermediate at the active site of the enzyme, any resonance overlap between the carbonyl group and the aromatic heterocycle would be lost, thereby unmasking the full hydrogen-bonding ability of the ring nitrogen atom. Hydrogen bond formation with the protonated imidazole of the active site His-57 would help to stabilize the tetrahedral complex and serve to compensate for the disruption of the conjugated system (Figure 5). This is analogous to the mechanism of peptide bond hydrolysis in which an amido nitrogen atom that is normally a hydrogen bond donor is transformed into a hydrogen bond acceptor upon for-

Table V. Kinetic Comparison of Electrophilic Carbonyl-Based Inhibitors

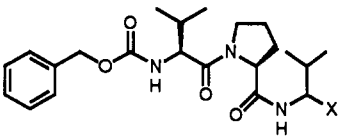

no.	X	K_i,[a] nM
17		8000
3		41
18		1.6[b]
1	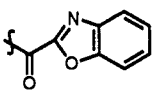	3.0
6	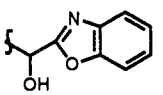	21000
15	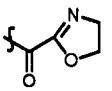	0.6

[a] Inhibition of HLE-catalyzed hydrolysis of the synthetic substrate MeO-Suc-Ala-Ala-Pro-Val-pNA at pH 7.8. [b] Reference 8.

(37) Fisher, E. *Ber. Dtsch. Chem. Ges.* **1894**, *27*, 2983–2993.

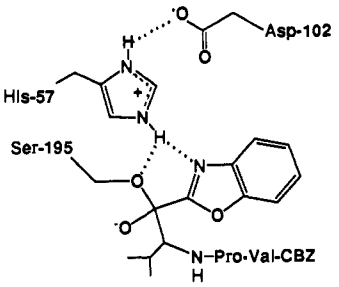

Figure 5. Conceptualized interaction between a peptidyl α-ketobenzoxazole and the catalytic triad in the active site of a serine proteinase. Hashed lines represent hydrogen bonds.

mation of the tetrahedral adduct, subsequently accepts a proton from His-57, and is released as part of the product amine.

Support for the hypothesis that the nitrogen atom of the α-ketoheterocycles interacts with an active site residue of the enzyme comes from a comparison of the inhibition constants and electronic properties of the benzoxazole **1** with those of the oxazoline **15**. A 2-benzoxazole ring (σ_I = 0.41)[38a] is much more electron withdrawing than a 2-oxazoline ring (σ_I = 0.32)[38b] and would therefore be expected to afford the more potent inhibitor due to the resulting increase in electrophilicity of the ketone carbonyl. Inconsistent with this expectation, the α-ketooxazoline **15** is 5 times more potent than the α-ketobenzoxazole **1** (Table V). However, since an oxazoline is a stronger hydrogen bond acceptor than the aromatic benzoxazole,[39] the α-ketooxazoline would be expected to form a tighter hydrogen bond between the ring heteroatom and the protonated His-57. If this hydrogen bond contributes significantly to the stability of the complex, the α-ketooxazoline would be predicted to be the more potent inhibitor, in agreement with the experimental results.

In order to confirm that the α-ketobenzoxazoles form a tetrahedral adduct with the active site Ser-195, as well as to obtain additional experimental evidence that the heterocyclic ring of these inhibitors participates in a hydrogen-bonding interaction with His-57, we endeavored to determine the X-ray crystal structure of an α-ketobenzoxazole–serine proteinase complex. At the time we began these studies, no crystal structure between HLE and a low molecular weight inhibitor had been reported. However, several X-ray structures of the complexes between PPE and peptidyl inhibitors had been solved.[20,21] Of the well-characterized serine proteinases, PPE is most similar to HLE.[36] The two enzymes share similar substrate specificity and have a 40% primary sequence homology. In addition, a comparison of the X-ray crystal structures of a number of PPE and HLE complexes revealed a surprising topological similarity between the enzymes, especially in their active site regions.[36] Therefore, the structural information obtained from a PPE–ketobenzoxazole complex will further our understanding of the mechanism of inhibition of both PPE and HLE by this class of inhibitors.

In the native PPE crystals used for the inhibitor soaking experiments, the enzyme S_4 subsite is blocked by a symmetry-related molecule. As a result, α-ketobenzoxazole **1** was not considered suitable for complex formation since its large benzyloxycarbonyl group extends into the S_4 pocket. Therefore, inhibitor **2**, with the small acetyl group at the N-terminus of the peptide, was chosen for the study. In addition, an alanine residue was incorporated into the P_3 position to allow comparison with other peptidyl inhibitor–PPE complexes. It was necessary to perform the X-ray experiment at a pH of 5.0 in order to maintain the integrity of the enzyme crystal.

The crystal structure of **2** bound to PPE clearly reveals the covalent attachment of the hydroxyl group of Ser-195 to the ketone carbonyl group of the inhibitor. The carbonyl carbon atom has rehybridized and possesses a tetrahedral geometry in the complex with the carbonyl oxygen atom positioned in the oxy anion hole. It has been theorized[40] that the tight binding nature of TFMK inhibitors to serine proteinases results from the ability of the trifluoromethyl group to increase the acidity of the hemiketal hydroxyl group such that it is ionized in the oxy anion hole and can thereby take maximum advantage of the stabilization afforded through hydrogen-bonding interactions with the NH of Ser-195 and Gly-193 in the oxy anion hole. Recently, the pK_a of the hemiketal oxygen atom of a peptidyl trifluoromethyl ketone bound to chymotrypsin was reported[40b] to be less than 4.0. The high acidity of the hemiketal oxygen atom results from a combination of ionic stabilization with the protonated His-57, the polar environment of the oxy anion hole, and the inductive effect of the CF_3 group. Crystallographically, this is reflected in the short interatomic distance between the hemiketal oxygen and the nitrogen atoms of the oxy anion hole: in the crystal structure of a peptidyl TFMK bound to PPE,[20] the distance is 2.97 Å to Ser-195 and 2.58 Å to Gly-193. In the current structure of ketobenzoxazole **2** bound to PPE, the distances of the hemiketal oxygen to the nitrogen atoms of Ser-195 and Gly-193 in the oxy anion hole are 2.56 and 2.65 Å, respectively. These short hydrogen bonds suggest that the tetrahedral adduct between the peptidyl α-ketobenzoxazole **2** and PPE exists as the hemiketal oxy anion.

The current complex of **2** bound to PPE also confirms the positive binding interaction between His-57 and the nitrogen atom of the benzoxazole ring. While it is not possible here to resolve the positions of protons by X-ray crystallography, the short interatomic distance between the two heteroatoms (2.81 Å) would be disfavored by a negative dipole interaction if not bridged by a proton. It is also not possible to distinguish between the nitrogen and oxygen atoms in the quasi-symmetrical benzoxazole ring. We have positioned the ring with the nitrogen atom directed toward His-57 since the oxygen atom of a 2-benzoxazole, which serves as a π-donor atom, is not expected to posses any hydrogen-bonding capability. π-Donor heteroatoms in general, and those in heterocycles in particular, do not function as hydrogen bond acceptors.[39] On the basis of the kinetic and crystallographic data presented here, we believe that the hydrogen bond between His-57 and the benzoxazole nitrogen contributes significantly to the stability of the complex. In addition to the stabilization which can be attributed to formation of a hydrogen bond within the active site, the hydrogen bonding of the heterocycle to the protonated histidine would help transmit the positive charge through the heterocyclic ring to the hemiketal oxygen atom, thereby stabilizing the oxy anion. This might account for the very short oxygen to nitrogen interatomic distances observed in the oxy anion hole. The structure–activity relationships we have developed[22] are consistent with the importance of this hydrogen bond: replacement of the benzoxazole ring with heterocycles possessing a nitrogen atom with greater basicity and/or hydrogen bond acceptor ability improves potency, even if the heterocycle is less electron withdrawing, such as the α-ketooxazoline **15**. *This is the only reported example of a reversible, mechanism-based inhibitor of a serine proteinase designed, and experimentally determined, to exploit the binding potential of both the histidine and serine of the catalytic triad.*

Finally, the current study shows that the binding of the inhibitor in the active site of PPE is the same as the productive forward binding expected of a natural peptidyl substrate. The valine residue in P_1 confirms that PPE can also accept branched residues like valine in the primary specificity site apart from other small unbranched nonpolar amino acid groups.[36] This is contrasted with the poor fit of isoleucine in a recently determined boronic acid complexed to PPE.[41] The proline at P_2 does not engage in any hydrogen-bonding interactions with the protein. It helps provide a complementary binding geometry to the active site region and restricts the number of binding modes. The alanine at P_3 forms

(38) (a) Taylor, P. J.; Wait, A. R. *J. Chem. Soc., Perkin Trans. 2* **1986**, 1765. (b) Taylor, P. J., personal communication.
(39) Abraham, M. H.; Duce, P. P.; Prior, D. V.; Barratt, D. G.; Morris, J. J.; Taylor, P. J. *J. Chem. Soc., Perkin Trans. 2* **1989**, 1355–1375.
(40) (a) Liang, T.-C.; Abeles, R. H. *Biochemistry* **1987**, *26*, 7603–7608. (b) Brady, K.; Liang, T.-C.; Abeles, R. H. *Biochemistry* **1989**, *28*, 9066–9070.
(41) Takahashi, L. H.; Radhakrishnan, R.; Rosenfield, R. E., Jr.; Meyer, E. F., Jr. *Biochemistry* **1989**, *28*, 7610–7617.

two short, tight hydrogen bonds to the enzyme and contributes to the β-pleated sheet arrangement.

Conclusion

The peptidyl α-ketobenzoxazoles represent a novel series of potent, mechanism-based inhibitors of both HLE and PPE. The α-ketobenzoxazoles interact with the active site of the elastases in a manner unique for a reversible heterocyclic inhibitor of serine proteinases, binding simultaneously to both the Ser-195 and His-57 of the catalytic triad. The combination of inhibitor design and kinetic evaluation supported by crystal structure analysis has proven to be a powerful process for understanding the mechanism of inhibition by the α-ketobenzoxazoles. Knowledge of the mode of inhibitor binding with PPE will be an extremely valuable aid in finding suitable peptidic, as well as nonpeptidic, substrates and inhibitors for other homologous enzymes for which the X-ray crystal structures have been determined, such as the physiologically important enzymes HLE[42] and thrombin.[43] The structural information from this study combined with the knowledge of the receptor binding geometries of serine proteinases will facilitate molecular modeling studies and aid the development of potent drugs to treat the diseases caused by these enzymes.

Experimental Section

General Methods. Analytical samples were homogeneous by TLC and afforded spectroscopic results consistent with the assigned structures. Proton NMR spectra were obtained by using either a Bruker WM-250 or AM-300 spectrometer. Chemical shifts are reported in parts per million relative to Me_4Si as internal standard. Mass spectra (MS) were recorded on a Kratos MS-80 instrument operating in the chemical ionization (DCI) mode. Elemental analyses for carbon, hydrogen, and nitrogen were determined by the ICI Americas Analytical Department on a Perkin-Elmer 241 elemental analyzer and are within ±0.4% of theory for the formulas given. Analytical thin-layer chromatography (TLC) was conducted on prelayered silica gel GHLF plates (Analtech, Newark, DE). Visualization of the plates was accomplished by using UV light, phosphomolybdic acid/ethanol and/or iodoplatinate charring. Analytical high-pressure liquid chromatography (HPLC) was conducted on a Zorbax ODS analytical column (4.6 mm × 25 cm) with a Beckman liquid chromatography 340 instrument. Flash chromatography was conducted on a Kieselgel 60, 230–400 mesh (E. Merck, Darmstadt, Germany). Solvents were either reagent or HPLC grade. Reactions were run at ambient temperature and under a nitrogen atmosphere unless otherwise noted. Solvent mixtures are expressed as volume/volume ratios. Solutions were evaporated under reduced pressure on a rotary evaporator. Starting materials were commercially available except for Cbz-Val-Pro-Val-H (**3**) and Cbz-Val-H (**7**), which were prepared as previously reported.[44] Cbz-Val-Pro-Val-CF_3 (**18**) was prepared as described in ref 45.

Compounds **4–6**, **8–10**, **13**, and **14** exist as mixtures of diastereomers epimeric at the two stereogenic centers α and β to the hydroxyl group. Compounds **1**, **2**, and **15** are epimeric at the carbon atom α to the ketone carbonyl group. When the proton NMR data for these diastereomeric compounds are reported, each individual resonance and its fractional integration are reported where the diastereomeric resonances for a particular proton are resolved.

(Benzyloxycarbonyl)-L-valyl-*N*-[1-[(2-benzoxazolyl)-carbonyl]-2-methylpropyl]-L-prolinamide (1). A solution of oxalyl chloride (0.27 mL, 3.1 mmol) in CH_2Cl_2 (10 mL) at −40 °C was treated with DMSO (0.44 mL, 6.2 mmol) and stirred for 15 min. Alcohol **6** (170 mg, 0.31 mmol) was added in CH_2Cl_2 (5 mL) and the resulting slurry stirred at −40 °C for 1 h. Triethylamine (2.2 mL, 15 mmol) was added and the mixture allowed to warm to ambient temperature and stirred an additional 3 h. The mixture was diluted with ethyl acetate, washed successively with 5% aqueous NaOCl and brine, dried [10% (w/w) K_2CO_3/Na_2SO_4] and evaporated. Purification by flash chromatography on silica gel (150 mL) eluting with acetone/hexanes (1:4) gave **2** as a white solid (108 mg, 64%) and as a 9:1 mixture of diastereomers epimeric at the carbon α to the ketone carbonyl: TLC, R_f = 0.36, THF/hexanes (35:65); HPLC, t_R = 6.84 min, FR = 2 mL/min, water/CH_3CN (1:1); MS (DCI) m/z = 549 (M + 1); ^1H NMR (250 MHz, DMSO-d_6/TFA) δ 0.88–1.03 (12 H, m), 1.84 (5 H, m), 2.43 (1 H, m), 3.59 (1 H, m), 3.74 (1 H, m), 4.06 (1 H, d, J = 8.3 Hz), 4.57 (1 H, m), 5.05 (1 H, AB q, J = 3.8 Hz), 5.12 (1 H, AB q, J = 3.8 Hz), 5.31 (0.9 H, d, J = 5.7 Hz), 5.37 (0.1 H, d, J = 5.0 Hz), 7.37 (5 H, br s), 7.55 (1 H, t, J = 7.6 Hz), 7.62 (1 H, t, J = 8.1 Hz), 7.89 (1 H, d, J = 8.1 Hz), 8.01 (1 H, d, J = 7.6 Hz); Anal. ($C_{30}H_{36}N_4O_6 \cdot 0.2H_2O$) C, H, N.

Acetyl-L-alanyl-*N*-[1-[(2-benzoxazolyl)carbonyl]-2-methylpropyl]-L-prolinamide (2). A solution of **13** (2.2 g, 5.0 mmol, assuming 100% yield of **9**) and 1-ethyl-3-[3-(dimethylamino)-propyl]carbodiimide hydrochloride (9.57 g, 50.0 mmol) in DMSO/toluene (1:1, 100 mL) was treated with dichloroacetic acid (2.60 mL, 20 mmol) and stirred for 16 h, and the solvent was evaporated. The product was isolated by flash chromatography on silica gel (300 mL), eluting with a CH_2Cl_2/methanol gradient (97:3, 95:5, 90:10; 850 mL). A second purification by flash chromatography on silica gel (200 mL), eluting with hexanes/acetone (1:1, 1400 mL), afforded **2** as a white solid (580 mg, 38% from **13**) and as a 9:1 mixture of diastereomers epimeric at the carbon α to the ketone carbonyl: TLC, R_f = 0.55, $CHCl_3$/methanol (95:5); HPLC, t_R = 6.74, FR = 0.6 mL/min, water/acetonitrile/tetrahydrofuran/trifluoroacetic acid (55:35:15:0.1); MS (DCI) m/z = 429 (M + 1); ^1H NMR (250 MHz, DMSO-d_6/TFA) δ 0.95 (3 H, d, J = 6.8 Hz), 1.00 (3 H, d, J = 6.8 Hz), 1.17 (2 H, d, J = 6.4 Hz), 1.75–2.13 (4 H, m), 1.84 (3 H, s), 2.38 (1 H, m), 3.58 (2 H, m), 4.35–4.10 (2 H, m), 5.25 (0.9 H, d, J = 5.6 Hz), 5.27 (0.1 H, d, J = 5.4 Hz), 7.56 (1 H, dt, J = 8.2, 1.4 Hz), 7.66 (1 H, dt, J = 7.6, 1.4 Hz), 7.91 (1 H, d, J = 8.2 Hz), 8.02 (1 H, d, J = 7.6 Hz); Anal. ($C_{22}H_{28}N_4O_5 \cdot 0.5H_2O$) C, H, N.

(Benzyloxycarbonyl)-L-valyl-*N*-[1-(cyanohydroxymethyl)-2-methylpropyl]-L-prolinamide (4). A solution of Cbz-Val-Pro-Val-H (**3**; 12.8 g, 29.7 mmol) in THF (128 mL) and water (154 mL) was treated with solid KCN (7.74 g, 119 mmol). The resulting mixture was stirred for 4.5 h and then partitioned between ethyl acetate and water. The aqueous layer was extracted with ethyl acetate, and the combined organic layers were washed with saturated $NaHCO_3$ and brine, dried (10% (w/w) K_2CO_3/Na_2SO_4), and evaporated to afford crude **4** (14.0 g), which was used without further purification: TLC, R_f = 0.17, acetone/hexanes (1:3); MS (DCI) m/z = 432 (M − HCN + 1); ^1H NMR (250 MHz, DMSO-d_6) δ 0.91 (12 H, m), 1.76–2.00 (6 H, m), 3.60 (1 H, m), 3.72 (1 H, m), 4.02 (1 H, m), 4.36–4.72 (2 H, m), 5.02 (2 H, m), 6.58 (1 H, m), 7.35 (6 H, m), 7.83 (0.5 H, d, J = 9.5 Hz), 7.95 (0.5 H, d, J = 9.5 Hz).

(Benzyloxycarbonyl)-L-valyl-*N*-[1-[(2-benzoxazolyl)hydroxymethyl]-2-methylpropyl]-L-prolinamide (6). A solution of anhydrous ethanol (1.22 mL, 20.7 mmol) in $CHCl_3$ (2 mL) at 0 °C was treated with acetyl chloride (1.24 mL, 17.4 mmol), followed by the addition of nitrile **4** (500 mg, 1.09 mmol) in $CHCl_3$ (3 mL). The mixture was allowed to warm to ambient temperature and stirred for 16 h. The solvent was evaporated, and the crude imidate **5** was taken up in ethanol (5 mL) and treated with *o*-aminophenol (119 mg, 1.09 mmol). The mixture was heated at 60 °C for 4 h, diluted with ethyl acetate, and washed with 1 N NaOH and brine, dried [10% (w/w) K_2CO_3/Na_2SO_4], and evaporated. Purification by flash chromatography on silica gel (200 mL), eluting with THF/hexanes (35:65, 2100 mL), gave **6** as a white solid (209 mg, 35%): TLC, R_f = 0.21, methanol/$CHCl_3$ (5:95); MS (DCI) m/z = 551 (M + 1); ^1H NMR (250 MHz, DMSO-

(42) Bode, W.; Wei, A.-Z.; Huber, R.; Meyer, E. F., Jr.; Travis, J.; Neumann, S. *EMBO J.* **1986**, *5*, 2453–2458.
(43) Bode, W.; Mayr, I.; Baumann, U.; Huber, R.; Stone, S. R.; Hofsteenge, J. *EMBO J.* **1989**, *8*, 3467–3475.
(44) Edwards, P. D.; Lewis, J. J.; Perkins, C. W.; Trainor, D. A.; Wildonger, R. A. European Patent Appl., Publication No. 0 291 234 A2, 1988.
(45) Schwartz, J. A.; Stein, M. M.; Wildonger, R. A.; Edwards, P. D.; Trainor, D. A. U.S. Patent 4 910 190, 1990.
(46) Jones, T. A. *J. Appl. Crystallogr.* **1978**, *11*, 268–272.

d_6/TFA) δ 0.84–1.05 (12 H, m), 1.52 (3 H, m), 1.90 (2.5 H, m), 2.28 (0.5 H, m), 3.41 (1 H, m), 3.62 (1 H, m), 3.86–4.38 (3 H, m), 4.75 (0.5 H, d, J = 8.6 Hz), 5.03 (2.5 H, M), 7.36 (7 H, m), 7.66 (2 H, m); Anal. ($C_{30}H_{38}N_4O_6$) C, H, N.

3-[(Benzyloxycarbonyl)amino]-2-hydroxy-4-methylpentanenitrile (8). A solution of Cbz-valinal (**7**; 67.2 g, 286 mmol) in methylene chloride (900 mL) was purged with nitrogen, treated with acetone cyanohydrin (79.0 mL, 858 mmol) followed by triethylamine (24.0 mL, 172 mmol), and stirred for 4 h. The solvent was evaporated and the residue taken up in ether. The ether solution was washed with brine (5×), dried ($MgSO_4$), and evaporated. The crude product was purified by flash chromatography on silica gel (1200 mL). Elution with acetone/hexanes (1:2, 4 L) gave **8** as a colorless, viscous oil (55.5 g, 74%): TLC, R_f = 0.48, CH_2Cl_2/methanol (95:5); ^{1}H NMR (250 MHz, DMSO-d_6/TFA) δ 0.77–0.93 (6 H, m), 1.83–2.10 (1 H, m), 3.55 (0.6 H, dd, J = 7.8, 4.4 Hz), 3.76 (0.4 H, dd, J = 9.7, 5.2 Hz), 4.36 (0.4 H, d, J = 9.7 Hz), 4.65 (0.6 H, d, J = 4.4 Hz), 5.09 (2 H, m), 7.36 (5 H, m).

2-[2-[(Benzyloxycarbonyl)amino]-1-hydroxy-3-methylbutyl]-benzoxazole (9). A solution of chloroform (40 mL) and absolute ethanol (36.7 mL, 624 mmol) at 0 °C under nitrogen was treated with acetyl chloride (40.5 mL, 567 mmol) dropwise over 15 min. Cyanohydrin **8** (4.97 g, 18.9 mmol) in chloroform (40 mL) was added, the mixture stirred at 0 °C for 1 h, and the solvent evaporated while maintaining the temperature at 25 °C or below. The crude imidate in anhydrous ethanol (95 mL) was treated with *o*-aminophenol (2.28 g, 20.8 mmol) and heated at reflux for 6 h, and the solvent was evaporated. The residue was taken up in ethyl acetate, washed successively with 1 N NaOH, 1 N HCl, saturated $NaHCO_3$, and brine, dried ($MgSO_4$), and evaporated. The crude product was purified by flash chromatography on silica gel (500 mL), eluting with a hexanes/acetone gradient (4:1, 3:1, 2:1; 2.1 L), to give **9** as a brown gum (3.35 g, 50%): TLC, R_f = 0.48, hexanes/acetone (2:1); MS (DCI) m/z = 355 (M + 1); ^{1}H NMR (300 MHz, DMSO-d_6/TFA) δ 0.88–1.00 (6 H, m), 1.77 (0.4 H, m), 2.27 (0.6 H, m), 3.71 (0.4 H, dd, J = 6.2, 4.5 Hz), 4.08 (0.6 H, dd, J = 9.3, 3.1 Hz), 4.72–5.02 (3 H, m), 7.00–7.42 (7 H, m), 7.72 (2 H, m).

2-(2-Amino-1-hydroxy-3-methylbutyl)benzoxazole (10). A solution of **9** (3.35 g, 9.45 mmol) in ethanol (50 mL) was treated with 10% Pd/C (950 mg) and shaken under a 50 psi atmosphere of hydrogen for 16 h. The mixture was filtered through diatomaceous earth and the solvent evaporated. The crude product was purified by flash chromatography on silica gel (150 mL), eluting with a CH_2Cl_2/methanol gradient (97:3, 94:6, 90:10; 1500 mL), to give **10** as a solid (2.02 g, 96%): TLC, R_f = 0.38, CH_2Cl_2/methanol (97:3); MS (DCI) m/z = 221 (M + 1), 203; ^{1}H NMR (250 MHz, DMSO-d_6) δ 0.82–0.96 (6 H, m), 1.47 (0.6 H, m), 1.97 (0.4 H, m), 2.85 (0.4 H, t, J = 5.9 Hz), 2.94 (0.6 H, dd, J = 8.4, 4.1 Hz), 4.54 (0.6 H, d, J = 8.4 Hz), 4.70 (0.4 H, d, J = 5.9 Hz), 7.39 (2 H, m), 7.71 (2 H, m).

Ac-Ala-Pro-OBn (11). A solution of *N*-acetyl-L-alanine (14.3 g, 109 mmol), L-proline benzyl ester hydrochloride (26.4 g, 109 mmol), HOBT (29.5 g, 218 mmol), and *N*-methylmorpholine (12.0 mL, 109 mmol) at 0 °C was treated with 1,3-dicyclohexylcarbodiimide (24.8 g, 120 mmol) portionwise over several minutes. The mixture was stirred at ambient temperature for 16 h and filtered, and the solvent was evaporated. The residue was taken up in ethyl acetate, filtered, and washed successively with saturated $NaHCO_3$, 1 N HCl, and brine, dried ($MgSO_4$), and evaporated. The crude product was purified by flash chromatography on silica gel (600 mL), eluting with ethyl acetate/methanol (98:2, 2.8 L), to give **11** as a colorless oil (32.4 g, 93%): TLC, R_f = 0.18, ethyl acetate/methanol (97:3); MS (DCI) m/z = 319 (M + 1); ^{1}H NMR (300 MHz, DMSO-d_6) δ 0.11 (3 H, d, J = 7.2 Hz), 0.76–1.97 (3 H, m), 1.86 (3 H, s), 2.17 (1 H, m), 3.55 (1 H, m), 3.66 (1 H, m), 4.37 (1 H, m), 4.51 (1 H, quintet, J = 7.2 Hz), 5.09 (1 H, AB q, J = 12.6 Hz), 5.12 (1 H, AB q, J = 12.6 Hz), 7.35 (5 H, m), 8.15 (1 H, d, J = 7.4 Hz).

Ac-Ala-Pro-OH (12). A solution of **11** (16.0 g, 50.3 mmol) in ethanol (250 mL), was treated with 10% Pd/C (5 g) and shaken under a 50 psi atmosphere of hydrogen for 16 h. The mixture was filtered through diatomaceous earth and the solvent evaporated to give **12** as a white solid (9.7 g, 84%): TLC, R_f = 0.02, CH_2Cl_2/methanol (97:3); MS (DCI) m/z = 229 (M + 1); ^{1}H NMR (300 MHz, DMSO-d_6) δ 1.18 (3 H, d, J = 7.2 Hz), 1.78–1.93 (3 H, m), 1.80 (3 H, s), 2.15 (1 H, m), 3.52 (1 H, m), 3.64 (1 H, m), 4.23 (1 H, dd, J = 8.6, 4.0 Hz), 4.59 (1 H, quintet, J = 7.2 Hz), 8.14 (1 H, d, J = 7.2 Hz).

Acetyl-L-alanyl-*N*-[1-[(2-benzoxazolyl)hydroxymethyl]-2-methylpropyl]-L-prolinamide (13). A solution of acid **12** (1.14 g, 5.00 mmol), amine **10** (1.10 g, 5.00 mmol), and HOBT (0.675 g, 5.00 mmol) in DMF (15 mL) was treated with 1-ethyl-3-[3-(dimethylamino)propyl]carbodiimide hydrochloride (1.05 g, 5.25 mmol) and stirred at room temperature for 16 h, and the solvent was evaporated. The crude product was dissolved in methanol and adsorbed onto diatomaceous earth (20 mL), and the solvent was evaporated. The residue was purified by flash chromatography on silica gel (200 mL), eluting with CH_2Cl_2/methanol/acetic acid (95:5:0.5, 1.6 L), to give **13** as a viscous oil (2.6 g >100%): TLC, R_f = 0.25, CH_2Cl_2/methanol/NH_4OH (95:5:1); MS (DCI) m/z = 431 (M + 1); ^{1}H NMR (250 MHz, DMSO-d_6/TFA) δ 0.87–1.21 (9 H, m), 1.30–2.30 (8 H, m), 3.21–3.60 (2 H, m), 3.9–5.1 (4 H, m), 7.36–7.76 (3 H, m), 7.99 (1 H, d, J = 10.7 Hz).

(Benzyloxycarbonyl)-L-valyl-*N*-[1-[(2-oxazolinyl)hydroxymethyl]-2-methylpropyl]-L-prolinamide (14). A suspension of imidate **5** (2.00 g, 3.70 mmol, prepared as described above from **4**) in CH_2Cl_2 (15 mL), was treated with 2-aminoethanol (452 mg, 7.39 mmol) and triethylamine (1.03 ml, 7.39 mmol) and the resulting homogeneous solution stirred at ambient temperature for 16 h. The reaction mixture was diluted with ethyl acetate and washed with 1 N NaOH and brine, dried ($MgSO_4$), and evaporated. Purification by flash chromatography on silica gel (200 mL), eluting with methanol/chloroform (3:97, 600 mL), gave **14** as a white solid (259 mg, 14%): TLC, R_f = 0.32, methanol/$CHCl_3$ (3:97); MS (DCI) m/z = 503 (M + 1); ^{1}H NMR (250 MHz, DMSO-d_6) δ 0.87 (12 H, m), 1.75–1.96 (6 H, m), 3.64 (4 H, m), 3.90–4.40 (4 H, m), 5.00 (2 H, m), 7.34 (7 H, m).

(Benzyloxycarbonyl)-L-valyl-*N*-[1-[(2-oxazolinyl)carbonyl]-2-methylpropyl]-L-prolinamide (15). A solution of oxalyl chloride (0.45 mL, 5.2 mmol) in CH_2Cl_2 (20 mL) at −40 °C was treated with DMSO (0.741 mL, 10.3 mmol) and stirred for 15 min. Alcohol **14** (259 mg, 0.52 mmol) was added in CH_2Cl_2 (7 mL) and the resulting slurry stirred at −40 °C for 1 h. Triethylamine (3.60 mL, 25.8 mmol) was added and the mixture allowed to warm to ambient temperature and stirred an additional 3 h. The mixture was diluted with ethyl acetate, washed successively with 5% aqueous NaOCl and brine, dried [10% (w/w) K_2CO_3/Na_2SO_4], and evaporated. Purification by flash chromatography on silica gel (150 mL), eluting with acetone/hexanes (35:65, 450 mL), followed by a second flash chromatography on silica gel (150 mL), eluting with methanol/chloroform (2:98, 360 mL), gave **15** as a white solid (58 mg, 22%): TLC, R_f = 0.54, methanol/chloroform (5:95); HPLC, t_R = 5.21 min, FR = 2 mL/min, water/CH_3CN (1:1); MS (DCI) m/z = 501 (M + 1); ^{1}H NMR (250 MHz, DMSO-d_6) δ 0.88 (12 H, m), 1.67–2.10 (5 H, m), 2.23 (1 H, m), 3.55 (1 H, m), 3.70 (1 H, m), 4.01 (3 H, m), 4.35 (2 H, m), 4.48 (1 H, m), 4.96 (3 H, m), 7.37 (5 H, m), 7.44 (1 H, d, J = 8.4 Hz), 8.16 (1 H, d, J = 7.5 Hz); Anal. ($C_{26}H_{36}N_4O_6 \cdot 0.75H_2O$) C, H, N.

(Benzyloxycarbonyl)-L-valyl-*N*-[1-(1-hydroxyethyl)-2-methylpropyl]-L-prolinamide (16). A solution of aldehyde **3** (538 mg, 1.25 mmol) in THF (30 mL) at −60 °C under nitrogen was treated dropwise with methyllithium (4.37 mL, 1.43 M, 6.24 mmol) and allowed to slowly warm to −30 °C. The mixture was stirred an additional 2 h and poured into saturated NH_4Cl, and the aqueous layer was extracted with ethyl acetate. The combined organic extracts were washed with water and brine, dried ($MgSO_4$), and evaporated. Purification by flash chromatography on silica gel, eluting with methanol/$CHCl_3$ (1:99), gave **16** as a white solid (135 mg, 56%): TLC, R_f = 0.22, methanol/$CHCl_3$ (1:50); MS (DCI) m/z = 448 (M + 1); ^{1}H NMR (DMSO-d_6) δ 0.93

(12 H, m), 1.72-2.10 (6 H, m), 3.16-4.44 (5 H, m), 4.99 (1 H, AB q, J = 12.6 Hz), 5.03 (1 H, AB q, J = 12.6 Hz), 7.33 (7 H, m).

(*S*)-(Benzyloxycarbonyl)-L-valyl-*N*-[1-acetyl-2-methylpropyl]-L-prolinamide (17). A solution of alcohol **16** (120 mg, 0.268 mmol) and 1-ethyl-3-[3-(dimethylamino)propyl]carbodiimide hydrochloride (514 mg, 2.68 mmol) in DMSO/toluene (1:1, 10 mL) was treated with dichloroacetic acid (0.090 mL, 1.1 mmol) and stirred for 16 h. The mixture was diluted with ethyl acetate, washed with 10% HCl and 10% HCl/brine (1:1), dried ($MgSO_4$), and evaporated. Purification by flash chromatography on silica gel, eluting with hexanes/acetone (4:1), gave **17** as a white solid (95 mg, 79%): TLC, R_f = 0.16, hexanes/acetone (4:1); HPLC, t_R = 8.98, FR = 2 mL/min, water/CH_3CN (3:2); MS (DCI) m/z = 446 (M + 1); ^1H NMR (DMSO-d_6) δ 0.97 (12 H, m), 1.70-2.20 (6 H, m), 2.06 (3 H, s), 3.58 (1 H, m), 3.71 (1 H, m), 4.07 (2 H, m), 4.44 (1 H, m), 4.99 (1 H, AB q, J = 12.6 Hz), 5.04 (1 H, AB q, J = 12.6 Hz), 7.35 (5 H, br s), 7.44 (1 H, d, J = 8.3 Hz), 8.07 (1 H, d, J = 8.0 Hz); Anal. ($C_{24}H_{35}N_3O_5$) C, H, N.

Kinetic Experiments. Kinetics of the inhibition of PPE or HLE by compounds **1-3**, **6**, **15**, and **17** were analyzed versus the synthetic substrate MeO-Suc-Ala-Ala-Pro-Val-pNA as discussed in the Kinetic Assay section of this paper. The inhibition constant of **18** was determined as previously reported.[8] HLE and PPE were obtained from Elastin Products and MeO-Suc-Ala-Ala-Pro-Val-pNA was purchased from Sigma. Progress curves were generated by recording the absorbance at 410 nm on a Cary 3 spectrophotometer for reaction solutions containing enzyme (7 nM HLE or 24 nM PPE), MeO-Suc-Ala-Ala-Pro-Val-pNA (160 μM for HLE, 500 μM for PPE), and several concentrations of inhibitor in either a pH 7.8 buffer (10 mM sodium phosphate, 500 mM NaCl) or pH 5.0 buffer (50 mM acetate, 500 mM NaCl) and 3.3% DMSO. Temperature was maintained at 25 °C with a Lauda K-RD circulating bath. Absorbances were continuously measured, digitized, and stored in a Compaq computer. Lineweaver-Burke plots were constructed from the reaction progress curves obtained as described above except that for the HLE assays the substrate concentration was varied between 25 and 600 μM, the inhibitor concentration was either zero or 15 nM, and the HLE concentration was 3 nM. For the PPE assays, the substrate concentration was varied between 0.125 and 1 mM, inhibitor concentration was either zero or 19 μM, and the PPE concentration was 48 nM.

Acknowledgment. We acknowledge the assistance of Dr. Charles Lerman and Dr. James Hall with the NMR experiments, Professor Robert Huber, MPIB, for the use of the FAST area detector, and support from the Robert A. Welch Foundation and The Texas Agricultural Experiment Station.

Synthesis and Structure Determination of the Adducts of the Potent Carcinogen 7,12-Dimethylbenz[*a*]anthracene and Deoxyribonucleosides Formed by Electrochemical Oxidation: Models for Metabolic Activation by One-Electron Oxidation

N. V. S RamaKrishna,[†] E. L. Cavalieri,*[,†] E. G. Rogan,[†] G. Dolnikowski,[‡] R. L. Cerny,[‡] M. L. Gross,[‡] H. Jeong,[§] R. Jankowiak,[§] and G. J. Small[§]

Contribution from the Eppley Institute for Research in Cancer, University of Nebraska Medical Center, 600 South 42nd Street, Omaha, Nebraska 68198-6805, Midwest Center for Mass Spectrometry, Department of Chemistry, University of Nebraska—Lincoln, Lincoln, Nebraska 68588, and Ames Laboratory-U.S. Department of Energy and Department of Chemistry, Iowa State University, Ames, Iowa 50011. *Received May 16, 1991*

Abstract: Anodic oxidation of 7,12-dimethylbenz[*a*]anthracene (7,12-DMBA) in the presence of dG yields four adducts and one oxygenated derivative of 7,12-DMBA: 7-methylbenz[*a*]anthracene (MBA)-12-CH_2-C8dG (13%), 7-MBA-12-CH_2-N7Gua (55%), 12-MBA-7-CH_2-N7Gua (12%), 7-MBA-12-CH_2-C8Gua (10%), and 7,12-$(CH_2OH)_2$-BA (10%). The first three are primary products of the electrochemical reaction, whereas the last two are secondary products. Binding occurs predominantly at the 12-CH_3 group of 7,12-DMBA and specifically to the N-7 and C-8 of Gua. On the other hand, anodic oxidation of 7,12-DMBA in the presence of dA gives only two detectable adducts: 7-MBA-12-CH_2-N7Ade (45%) and 12-MBA-7-CH_2-N3Ade (55%). Binding at the 12-CH_3 group is specific for the N-7 of Ade, whereas the 7-CH_3 group of 7,12-DMBA is specific for the N-3 of Ade. Structures of the adducts were elucidated by NMR and fast atom bombardment tandem mass spectrometry (FAB MS/MS). The adducts were also investigated by fluorescence line narrowing spectroscopy (FLNS). Both the FAB MS/MS and FLNS techniques can be used to distinguish between the adducts formed at the 7-CH_3 and 12-CH_3 groups of 7,12-DMBA (i.e., between 7-MBA-12-CH_2-N7Gua and 12-MBA-7-CH_2-N7Gua and between 7-MBA-12-CH_2-N7Gua and 7-MBA-12-CH_2-C8Gua). FLNS can distinguish 12-MBA-7-CH_2-N3Ade from 7-MBA-12-CH_2-N7Ade. On the other hand, the distinction between 7-MBA-12-CH_2-C8Gua and 7-MBA-12-CH_2-C8dG is straightforward by FAB MS but very difficult by FLNS. The electrochemical synthesis not only provides a demonstration of the specific reactivity of nucleosides and 7,12-DMBA under oxidizing conditions but is also a source of the necessary reference materials for studying the 7,12-DMBA-DNA adducts formed in biological systems. Furthermore, the analytical methodology is now appropriate for supporting in vivo studies of 7,12-DMBA-DNA adducts. A mechanism is proposed, although there are not sufficient data to prove it.

Introduction

Elucidation of the mechanisms of activation of polycyclic aromatic hydrocarbons (PAH) is central to an understanding of the process of tumor initiation and the design of preventive strategies. A powerful approach to this problem is to identify the structure of PAH-DNA adducts. Studies thus far point to two major mechanisms of activation: one-electron oxidation to form intermediate radical cations[1-4] and monooxygenation to produce

* Author to whom correspondence should be addressed.
† Eppley Institute for Research in Cancer.
‡ Midwest Center for Mass Spectrometry.
§ Iowa State University.

(1) Cavalieri, E.; Rogan, E. In *Free Radicals in Biology*; Pryor, W. A., Ed.; Academic: New York, 1984; Vol. VI, pp 323-369.

0002-7863/92/1514-1863$03.00/0